EQUIVALENT GRAPHICAL SOLUTIONS OF TERMINATED CONJUGATELY CHARACTERISTIC-IMPEDANCE TRANSMISSION LINES WITH NON-NEGATIVE AND CORRESPONDING NEGATIVE CHARACTERISTIC RESISTANCES

D. Torrungrueng and S. Lamultree

Department of Electrical and Electronic Engineering
Faculty of Engineering and Technology
Asian University
Chon Buri, 20250, Thailand

Abstract—This paper presents the graphical solutions of conjugately characteristic-impedance transmission lines (CCITLs) implemented by periodically loaded lossless transmission lines (TLs), which can exhibit both non-negative (NNCR) and negative characteristic resistances (NCR) with the corresponding propagation constants. The standard T-chart and the extended T-chart are employed to solve CCITL problems with NNCR and NCR cases respectively, depending on the argument of CCITL characteristic impedances. The range of plotting of the standard T-chart and the extended T-chart is always inside or on the unit circle, and always outside or on the unit circle of the voltage reflection coefficient plane, respectively. Two examples of finite periodic TL structures providing both NNCR and NCR cases are given. It is found that both T-charts provide the same input impedance of the corresponding CCITLs as expected, and the standard T-chart is more familiar and easier to deal with.

1. INTRODUCTION

One class of transmission lines (TLs), called conjugately characteristic-impedance transmission lines (CCITLs), has been introduced recently in the literature [1–7]. By definition, a CCITL possesses conjugate characteristic impedances $Z_0^{\pm}$ of waves propagating in the opposite directions along the transmission line. Examples of CCITLs are


Corresponding author: D. Torrungrueng (dtg@asianust.ac.th).

reciprocal lossless uniform TLs, nonreciprocal lossless uniform TLs [8–10], exponentially tapered lossless nonuniform TLs [2, 11, 12] and periodically loaded lossless TLs operated in passband [13–18]. Using the $ABCD$ matrix technique, it can be shown that the equation of the input impedance at each terminal of loaded finite lossless periodic structures is in the same form as that of CCITLs [4]. Thus, CCITLs can be conveniently implemented using periodically loaded lossless TLs in practice. It should be pointed out that the analytical approach for solving problems associated with CCITLs usually provides complex formulae. Thus, graphical tools are usually needed to simplify the analysis and design of CCITLs.

Recently, the graphical tools used in the analysis and design of CCITLs, called T-charts [1, 7] have been invented and applied to solve problems associated with CCITLs effectively. One can imagine that T-charts are a generalized version of the standard Smith chart developed for CCITLs. It is found that the T-chart generally depends on the phase angle ϕ associated with the effective characteristic impedances of CCITLs. As the parameters of CCITLs change, T-charts will be changed accordingly as well. Thus, T-charts will be effectively employed to simplify the analysis and design of CCITLs.

In the literature [5, 6], it is interestingly found that CCITLs can exhibit both non-negative (NNCR) ($\mathrm{Re}\{Z_0^{\pm}\} \geq 0$) and negative characteristic resistances (NCR) ($\mathrm{Re}\{Z_0^{\pm}\} < 0$) if the operating frequency is chosen appropriately. It should be pointed out that the standard T-chart can be applied for CCITLs with the NNCR case only [1], while the extended T-chart can treat the CCITL problems associated with the NCR case [7]. Interestingly, it has been recently found that both NNCR and NCR cases always exist in the same passbands by employing the analysis based on the short-circuited and open-circuited terminations for determining $Z_0^{\pm}$ and β of equivalent CCITLs [6]. Thus, the graphical solutions for the standard T-chart and the extended T-chart for equivalent CCITLs, with NNCR and corresponding NCR cases respectively, are expected to be identical. In this paper, graphical solutions based on both T-charts are employed to confirm this fact by determining the input impedances of terminated equivalent CCITLs.

The organization of this paper is as follows. Section 2 presents the theory of CCITLs associated with terminated finite lossless reciprocal periodic TL structures. Numerical results illustrating both NNCR and NCR cases are shown in Section 3. Finally, conclusions are presented in Section 4.
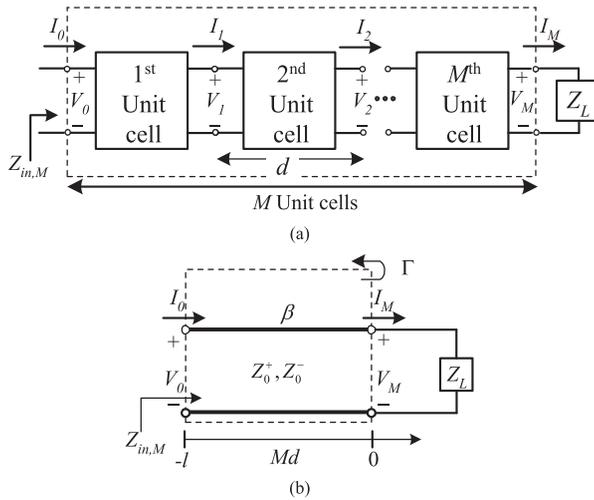
Figure 1. Models of: (a) a finite lossless reciprocal periodic TL structure of M unit cells terminated in a passive load impedance Z_L and (b) an equivalent CCITL terminated in Z_L.

2. THEORY OF CCITLS

The theory of CCITLs associated with terminated finite lossless reciprocal periodic TL structures is provided in this section. Fig. 1(a) shows a model of finite periodic TL structures of M unit cells terminated in a passive load impedance Z_L. Each unit cell of length d is characterized by its transmission ($ABCD$) matrix. The input impedance of the finite periodic structure of M unit cells is defined as $Z_{in,M}$. In [4], Fig. 1(a) can be viewed as a CCITL model of length $l = Md$ as shown in Fig. 1(b) possessing the propagation constant β, with corresponding characteristic impedances, Z_0^+ and Z_0^-, for waves propagating in the forward and reverse directions, respectively. By definition of CCITLs, Z_0^+ and Z_0^- are complex conjugate of each other, and β is the same for both forward and reverse waves for reciprocal periodic TL structures. In this model, only the terminal quantities are of interest without considering any physical quantities inside periodic TL structures. The traveling wave equations for the phasor voltage V_m and the phasor current I_m in the passsbands at the terminal of the mth unit cell (where $m = 1, 2, \ldots, M$) can be written as [11]

$$V_m = V_0^+ e^{-jm\beta d} + V_0^- e^{jm\beta d}, \qquad (1)$$

$$I_m = \frac{V_0^+}{Z_0^+} e^{-jm\beta d} - \frac{V_0^-}{Z_0^-} e^{jm\beta d}, \tag{2}$$

where V_0^+ and V_0^- are defined as the amplitudes of the incident and reflected voltage waves referenced at the input of the finite periodic TL structure, respectively.

Using the $ABCD$ matrix technique, $Z_0^\pm$ can be expressed in terms of the total $ABCD$ parameters of the unit cell of interest as [4]

$$Z_0^\pm = \frac{\mp 2B}{A - D \mp j\sqrt{4 - (A+D)^2}}, \tag{3}$$

where they are complex conjugate to each other in the passbands only. For convenience in analysis, $Z_0^\pm$ are defined in the polar form as

$$Z_0^\pm = |Z_0| e^{\mp j\phi}, \tag{4}$$

where $|Z_0|$ and ϕ are the magnitude and the argument of Z_0^-, respectively. For the NNCR case, (4) implies that the argument ϕ must lie in the following range:

$$-90^\circ \le \phi \le 90^\circ, \tag{5}$$

where $\cos\phi \ge 0$ in this range. For the NCR case, the valid range of the argument ϕ is

$$-180^\circ < \phi < -90^\circ \quad \text{and} \quad 90^\circ < \phi \le 180^\circ, \tag{6}$$

where $\cos\phi < 0$. Two examples of terminated finite periodic TL structures exhibiting both NNCR and NCR cases will be illustrated in Section 3.

In (1) and (2), β can be determined from the following dispersion relation [11]:

$$\cos\beta d = \frac{A+D}{2}. \tag{7}$$

Note that the magnitude of the right-hand side of (7) is always less than or equal to unity in passbands; i.e., β is *real*. As shown in [4], the input impedance $Z_{in,M}$ (see Fig. 1(a)) of the terminated finite periodic TL structure of M unit cells is given by

$$Z_{in,M} = Z_0^+ Z_0^- \frac{1 + \Gamma e^{-j2M\beta d}}{Z_0^- - Z_0^+ \Gamma e^{-j2M\beta d}}, \tag{8}$$

where Γ is the voltage reflection coefficient at the load mathematically given as

$$\Gamma = \frac{Z_L Z_0^- - Z_0^+ Z_0^-}{Z_L Z_0^+ + Z_0^+ Z_0^-}. \tag{9}$$

From (8) and (9), it is obvious that the matching condition resulting in $Z_{inM} = Z_L$ for periodic TL structures can be obtained when $Z_L = Z_0^+$ for the NNCR case ($\mathrm{Re}\{Z_0^\pm\} \geq 0$) and $Z_L = -Z_0^-$ for the NCR case ($\mathrm{Re}\{Z_0^\pm\} < 0$); i.e., the magnitude of Γ is equal to zero and approaches infinity, respectively. Moreover, $|\Gamma|$ is always less than or equal to unity for the NNCR case, and always greater than or equal to unity for the NCR case [6]. However, associated powers for both cases are still conserved for passive load terminations as also shown in [6].

Recently, it has been shown that CCITL parameters (Z_0^+, Z_0^- and β) can be determined rigorously by using the analysis based on short-circuited and open-circuited terminations [6], which is briefly described below. Fig. 1(b) with $M = 1$ illustrates an equivalent CCITL model of a single unit cell terminated in a passive load impedance Z_L at its right terminal, where $Z_{in,L} = Z_{in,M}$ ($M = 1$) is the input impedance seen from the left terminal of the CCITL. It should be pointed out that only one unit cell ($M = 1$) is considered in determining CCITL parameters of periodic TL structures since the $ABCD$ matrix of each unit cell of periodic TL structures is identical, and the single unit cell contains all needed information for computing CCITL parameters. For the short-circuited load ($Z_L = 0$), $Z_{in,L}$ can be computed using (8) with $M = 1$ as

$$Z_{in,L}\Big|_{Z_L=0} = Z_0^+ Z_0^- \frac{1 - e^{-j2\beta d}}{Z_0^- + Z_0^+ e^{-j2\beta d}}. \tag{10}$$

For the open-circuited load ($|Z_L| \to \infty$), $Z_{in,L}$ is given as

$$Z_{in,L}\Big|_{|Z_L|\to\infty} = \frac{Z_0^+ Z_0^- e^{-j2\beta d}}{1 - e^{-j2\beta d}}. \tag{11}$$

One more equation is needed in uniquely solving for Z_0^+, Z_0^- and β, and can be obtained from the interchanging Z_L in Fig. 1(b) to its left terminal instead. Then, considering the short-circuited load yields another equation. The input impedance ($Z_{in,R}$) seen from the right terminal of the short-circuited CCITL can be found as

$$Z_{in,R}\Big|_{Z_L=0} = Z_0^+ Z_0^- \frac{1 - e^{-j2\beta d}}{Z_0^+ + Z_0^- e^{-j2\beta d}}. \tag{12}$$

In the CCITL system, observing from the left terminal of the CCITL, it is found that Z_0^+ and Z_0^- are the characteristic impedances for waves propagating in the forward and reverse directions, respectively. On the other hand, observing from the right one, waves propagating in the forward and reverse directions possess Z_0^- and Z_0^+, respectively. Thus, interchanging of Z_0^+ and Z_0^- in (8) and (9) with $Z_L = 0$, $Z_{in,R}$ can be written compactly as shown in (12).

Solving (10), (11) and (12) simultaneously, Z_0^+, Z_0^- and β can be determined analytically as follows [6]:

$$Z_0^- = \frac{-Q_2 \pm \sqrt{Q_2^2 + 4Q_1}}{2}, \tag{13}$$

$$Z_0^+ = Z_0^- + Q_2, \tag{14}$$

and β can be determined from

$$e^{-j2\beta d} = \frac{1 - R_1 Z_0^-}{1 + R_1 Z_0^+}. \tag{15}$$

Note that Q_1, Q_2 and R_1 in the above equations are defined in terms of $Z_{in,L}$ and $Z_{in,R}$ under short-circuited and/or open-circuited terminations as

$$Q_1 \equiv Z_{in,L}\Big|_{|Z_L| \to \infty} \cdot Z_{in,R}\Big|_{Z_L = 0}, \tag{16}$$

$$Q_2 = Z_{in,L}\Big|_{|Z_L| \to \infty} - \frac{1}{R_1}, \tag{17}$$

$$R_1 = \frac{Z_{in,L}\Big|_{Z_L = 0}}{Z_{in,L}\Big|_{|Z_L| \to \infty} \cdot Z_{in,R}\Big|_{Z_L = 0}}. \tag{18}$$

It should be pointed out that there are two sets of solutions for $Z_0^\pm$ and β from the above analysis as seen in (13). It is found that one solution yields the NNCR case; i.e., $Z_0^\pm = R \pm jX$ with $\beta = T + \frac{n\pi}{d}$ (for $-\pi < Td \le \pi$), where R, X and T are real, n is a nonnegative integer (see [6] for more details of choosing appropriate values of n), and $R \ge 0$. Another solution yields the NCR case; i.e., $Z_0^\pm = -R_0 \pm jX$ with $\beta = -T + \frac{n\pi}{d}$, where $R_0 = R$ when $R \ne 0$, and $R_0 > 0$. In [6], it is shown rigorously that equivalent CCITL models based on both NNCR and corresponding NCR cases are equivalent; i.e., they provide the identical $ABCD$ matrix of the unit cell of interest. In the next section, two examples of terminated finite periodic TL structures exhibiting both NNCR and NCR cases are provided. In addition, graphical solutions based on the standard T-chart and the extended T-chart of these specific examples are employed to confirm that both CCITL models are equivalent.

3. NUMERICAL RESULTS

Figure 2 illustrates a finite periodic TL structure implemented by a multi-section transmission line (MSTL) of coplanar waveguides (CPW)

[19, 20]. An MSTL with a three-section CPW is analyzed and designed using the Agilent Genesys EDA software [21]. Equivalent CCITL parameters $Z_0^{\pm}$ and β of MSTL can be determined rigorously using the theory in Section 2. The three-section CPW printed on the printed board circuit (PCB) with dielectric constant of 3, substrate height of 0.75 mm and conductor thickness of 0.035 mm. It consists of center conductor width w, slot width s, ground plane width g and center conductor length L as shown in Fig. 2(a).


(a)   (b)
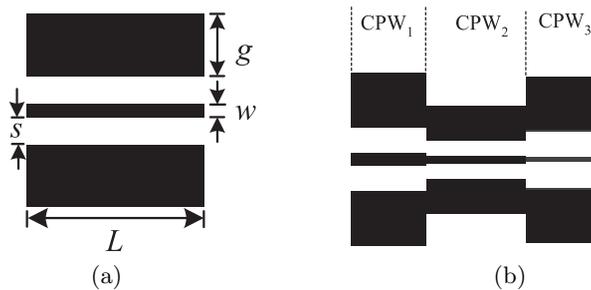
Figure 2. A model of MSTL: (a) A CPW and (b) Three-section CPW.

Sizes of each CPW are tabulated in Table 1. The frequency of interest ranges from 0.5 to 5 GHz. Note that a unity of M ($M = 1$) is employed in this paper, and the length d of the unit cell of Fig. 1(b) is 50 mm. Using (3) and (7), it is found that β satisfying $|\cos \beta d| \leq 1$ is in the 1st passband (0.5–2.413 GHz) and the 2nd passband (2.795–5 GHz), corresponding to the NNCR and NCR cases respectively, as shown in Fig. 3. Note that the complex value of β is observed in the stopband (between 2.413 GHz and 2.795 GHz). Only β in the passbands is plotted.

Table 1. Physical sizes of CPWs.

Section	w (mm)	s (mm)	g (mm)	L (mm)
CPW$_1$	2.5	5.0	11.0	15.0
CPW$_2$	1.5	3.0	7.0	20.0
CPW$_3$	1.0	5.0	11.0	15.0

Using (3), Figs. 4 and 5 plot the magnitudes and arguments of $Z_0^{\pm}$ versus frequency, respectively. In Fig. 5, ϕ^+ and ϕ^- denote the arguments of Z_0^+ and Z_0^-, respectively. It is observed that Z_0^+ and Z_0^- are complex conjugate of each other in the passbands only. In addition, this MSTL exhibits the NNCR and NCR in the 1st passband
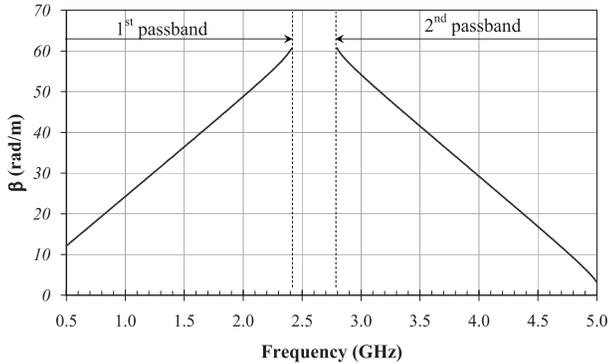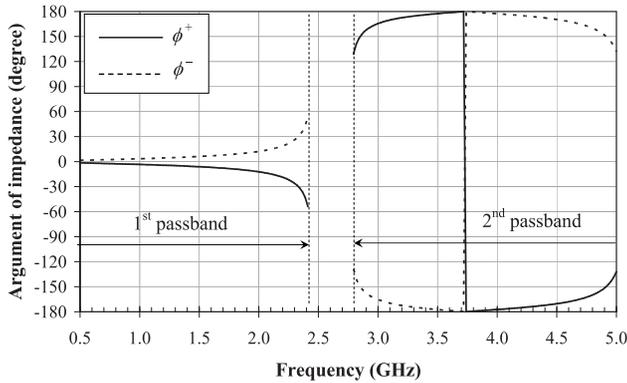
Figure 3. β versus frequency.
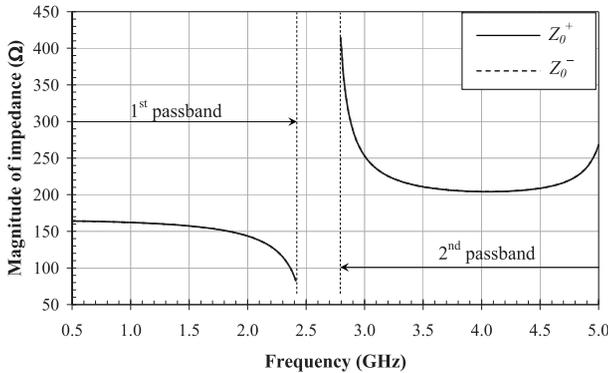
Figure 4. Magnitudes of Z_0^+ and Z_0^- versus frequency.

and the 2nd passband respectively, as shown in Fig. 5. Away from the passbands (i.e., stopbands), it is found that $Z_0^{\pm}$ are purely imaginary with different magnitudes.

Next, it is of interest to determine the input impedance $Z_{in,M}$ of the MSTL terminated in the load impedance Z_L of $50\,\Omega$ at the operating frequency of $3\,\text{GHz}$ using the standard analysis based on the $ABCD$ matrix technique (see (3) and (7)) and the analysis based on short-circuited and open-circuited terminations (see (13) to (15)). At this operating frequency, using the standard analysis based on the $ABCD$ matrix technique, $Z_0^{\pm} = -244.681 \pm j63.073\,\Omega$ and $\beta = 54.186\,\text{rad/m}$ (corresponding to the NCR case) are obtained as shown in Figs. 4 and 5. However, the analysis based on short-circuited and open-circuited terminations for the NNCR case provides $Z_0^{\pm} =$

Figure 5. ϕ^+ and ϕ^- versus frequency.

$244.681 \pm j63.073\,\Omega$ and $\beta = -54.186 + \frac{n\pi}{d}$ (using $\beta = 71.478\,\text{rad/m}$ (for $n = 2$)) [6]. In addition, CCITL parameters of the corresponding NCR case are $Z_0^\pm = -244.681 \pm j63.073\,\Omega$ and $\beta = 54.186\,\text{rad/m}$. It should be pointed out that the analysis based on the short-circuited and open-circuited terminations always provides both NNCR and NCR cases existing in the same passbands while the standard analysis based on the $ABCD$ matrix technique (see (3)) always provides either NNCR or NCR cases only in a passband; e.g., considering $Z_0^\pm$ at $3\,\text{GHz}$ for both methods. Using (8) and (9), $Z_{in,M}$ of the MSTL with the NNCR and corresponding NCR cases can be readily calculated. It is found that they provide the identical $Z_{in,M}$ of $48.069 + j103.551\,\Omega$ with different $|\Gamma|$ of 0.679 and 1.473 for the NNCR and corresponding NCR cases respectively, as expected.

Applying both T-charts to determine $Z_{in,M}$, the plots of the normalized input impedances $z_{in,M}$ of the standard T-chart [1] for $\phi = -14.46°$ and the extended T-chart [7] for $\phi = -165.55°$ are shown in Figs. 6(a) and 6(b), respectively. Note that both T-charts depend on the argument of characteristic impedance ϕ. For passive loads, the valid regions of the standard T-chart and the extended T-chart are on or inside, and on or outside the unit circle in the Γ plane, respectively. In this paper, impedances are normalized with respect to $|Z_0|$. To determine $Z_{in,M}$ of the NNCR case, the normalized load impedance z_L of $50/|Z_0| = 0.198$ is plotted on the standard T-chart as shown in Fig. 6(a). Starting from the z_L point, the normalized input impedance $z_{in,M}$ can be found graphically by rotating the z_L point clockwise an amount of $2\beta d$ along the circular path passing through z_L. However, it moves around the circle more than $360°$. Thus, only the circular path of an amount of $2\beta d - 2\pi$ is plotted in Fig. 6(a). This
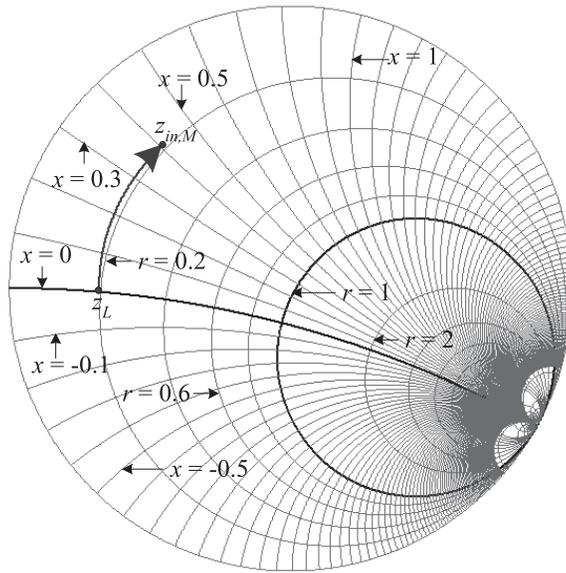
(a)
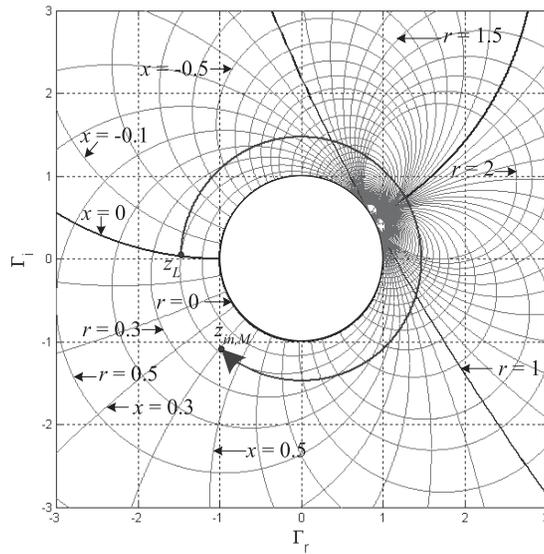
(b)

Figure 6. Determination of $Z_{in,M}$ of the MSTL: (a) NNCR case, (b) NCR case.

is due to the periodic property of this TL for its impedance to repeat itself for every half-wavelength. Therefore, the $z_{in,M}$ point can be read as $r = 0.19$ and $x = 0.41$, and the input impedance $Z_{in,M}$ can be computed as $z_{in,M}|Z_0|$, which is equal to $48.01 + j103.60\,\Omega$. In addition, Fig. 6(b) illustrates the determination of $z_{in,M}$ of the corresponding NCR case on the extended T-chart. Following the similar procedure as the previous case, $z_{in,M}$ can be determined graphically by starting from the normalized $z_L = 0.198$ and rotating in the clockwise direction by an amount of $2\beta d$ along the circular path passing through z_L. Finally, $z_{in,M}$ can be found at $r = 0.19$ and $x = 0.41$ with $Z_{in,M}$ of $48.01 + j103.60\,\Omega$, which is identical to the result of the NNCR case. Comparing the graphical solutions of $Z_{in,M}$ to that based on (8) and (9), it is found that they are in excellent agreement.

In addition to computing the MSTL with only a single unit cell ($M = 1$), the input impedance $Z_{in,M}$ of terminated five identical unit cells ($M = 5$ and $Z_L = 50\,\Omega$) of three-section CPW in cascade connection at $3\,\mathrm{GHz}$, used as an example for practical applications, can be determined by using these T charts showing their convenience in usage of multiple unit cells. Using (8) and (9) of the $ABCD$ matrix technique, $Z_{in,M}$ of $341.563 - j462.950\,\Omega$ can be obtained using the same CCITL parameters ($Z_0^{\pm}, \beta$) of the unit cell as in the previous example. Furthermore, applying both T-charts to determine $Z_{in,M}$ for $M = 5$, the plots of the normalized input impedances $z_{in,M}$ of the standard T-chart for $\phi = -14.46°$ and the extended T-chart for $\phi = -165.55°$ are shown in Figs. 7(a) and 7(b), respectively. In Fig. 7(a), starting from the z_L point, the normalized input impedance $z_{in,M}$ can be found graphically by rotating the z_L point clockwise an amount of $2M\beta d$ along the circular path passing through z_L. However, only the circular path of an amount of $2M\beta d - 2M\pi$ is plotted in Fig. 7(a) due to the periodic property of this TL. Therefore, the $z_{in,M}$ point can be finally read as $r = 1.35$ and $x = -1.83$ resulting in the input impedance $Z_{in,M}$ of $341.12 - j462.40\,\Omega$. In addition, Fig. 7(b) illustrates the determination of $z_{in,M}$ of the corresponding NCR case on the extended T-chart. Following the similar procedure as the previous case, $z_{in,M}$ can be determined graphically by starting from the normalized $z_L = 0.198$ and rotating in the clockwise direction by an amount of $2M\beta d$ along the circular path passing through z_L. Only the circular path of an amount of $2M\beta d - 2(M-1)\pi$ is plotted in Fig. 7(b). Finally, $z_{in,M}$ can be found at $r = 1.35$ and $x = -1.83$ corresponding to $Z_{in,M}$ of $341.12 - j462.40\,\Omega$, which is identical to the result of the NNCR case. Again, they are in excellent agreement with $Z_{in,M}$ computed using (8) and (9) above.
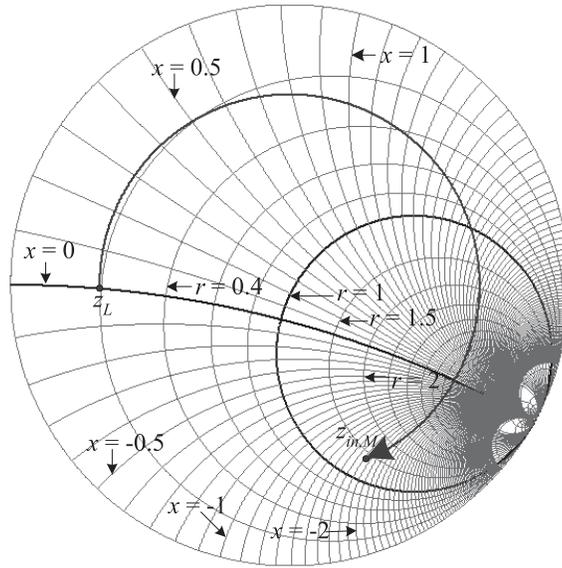
(a)
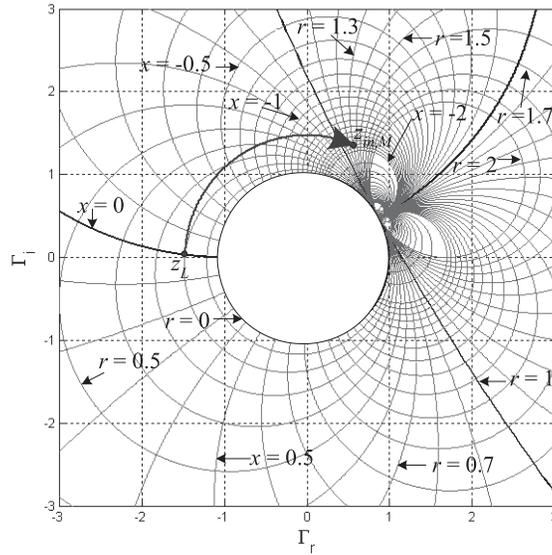
(b)

Figure 7. Determination of $z_{in,M}$ of the MSTL with $M = 5$: (a) NNCR case, (b) NCR case.

4. CONCLUSIONS

Two identical graphical solutions of a type of CCITLs, lossless periodic TL structures implemented by the three-section CPW as a unit cell providing both NNCR and NCR cases, are presented in this paper. It is found that the magnitude of the voltage reflection coefficient is always less than or equal to unity for the NNCR case, and always greater than or equal to unity for the NCR case. The standard T-chart and the extended one are dependent on the argument of the characteristic impedances of CCITLs, and they are employed to effectively and intuitively solve CCITL problems with NNCR and NCR cases, respectively. At the selected frequency in passbands, the ranges of plotting the standard T-chart for the NNCR case and the extended one for the NCR case are always inside or on the unit circle, and outside or on the unit circle of Γ plane, respectively. Nevertheless, the input impedances of the equivalent terminated CCITLs with the NNCR and corresponding NCR cases, obtained by using appropriated T-charts, are almost identical to that calculating directly from (8) and (9) for both single and five unit cells of the three-section CPW. Due to the fact that the NNCR case is more familiar and easier to deal with, the corresponding NCR case can always convert into the NNCR case, then the standard T-chart can be employed to solve problems effectively.

REFERENCES

1. Torrungrueng, D. and C. Thimaporn, "A generalized ZY Smith chart for solving nonreciprocal uniform transmission-line problems," *Microwave and Optical Technology Letters*, Vol. 40, No. 1, 57–61, 2004.

2. Torrungrueng, D. and C. Thimaporn, "Application of the T-chart for solving exponentially tapered lossless nonuniform transmission-line problems," *Microwave and Optical Technology Letters*, Vol. 45, No. 5, 402–406, 2005.

3. Torrungrueng, D. and C. Thimaporn, "Applications of the ZY T-chart for nonreciprocal stub tuners," *Microwave and Optical Technology Letters*, Vol. 45, No. 3, 259–262, 2005.

4. Torrungrueng, D., C. Thimaporn, and N. Chamnandechakun, "An application of the T-chart for solving problems associated with terminated finite lossless periodic structures," *Microwave and Optical Technology Letters*, Vol. 47, No. 6, 594–597, 2005.

5. Lamultree, S. and D. Torrungrueng, "On the characteristics of conjugately characteristic-impedance transmission lines with

active characteristic impedance," *The proceedings of the 2006 Asia-Pacific Microwave Conference*, Vol. 1, 225–228, 2006.

6. Torrungrueng, D., S. Lamultree, C. Phongcharoenpanich, and M. Krairiksh, "An in-depth analysis of reciprocal periodic structures of transmission lines," Accepted to publish in *IET Microwaves, Antennas & Propagation*, 2009.

7. Chou, P. Y. and D. Torrungrueng, "An extended ZY T-chart for conjugately characteristic-impedance transmission lines with active characteristic impedances," *Microwave and Optical Technology Letters*, Vol. 40, No. 1, 57–61, 2004.

8. Kharadly, M. M. Z., "Periodically loaded nonreciprocal transmission lines for phase-shifter applications," *IEEE Transactions on Microwave Theory and Techniques*, Vol. 22, No. 6, 635–640, 1974.

9. Lindell, I. V., M. E. Valtonen, and A. H. Sihvola, "Theory of nonreciprocal and nonsymmetric uniform transmission lines," *IEEE Transactions on Microwave Theory and Techniques*, Vol. 42, No. 2, 291–297, 1994.

10. Lindell, I. V. and A. H. Sihvola, "Duality transformation for nonreciprocal and nonsymmetric transmission lines," *IEEE Transactions on Microwave Theory and Techniques*, Vol. 45, No. 1, 129–131, 1997.

11. Pozar, D. M., *Microwave Engineering*, 2nd edition, John Wiley & Sons, 1998.

12. Wu, Y. and Y. Liu, "Standard Smith chart approach to solve exponential tapered nonuniform transmission line problems," *Journal of Electromagnetic Waves and Applications*, Vol. 22, 1639–1646, 2008.

13. Zhu, Y. and R. Lee, "TVFEM analysis of periodic structures for radiation and scattering," *Progress In Electromagnetics Research*, PIER 25, 1–22, 2000.

14. Khalaj-Amirhosseini, M., "Analysis of periodic and aperiodic coupled nonuniform transmission lines using the Fourier series expansion," *Progress In Electromagnetics Research*, PIER 65, 15–26, 2006.

15. Lu, W. and T.-J. Cui, "Efficient method for full-wave analysis of large-scale finite-sized periodic structures," *Journal of Electromagnetic Waves and Applications*, Vol. 21, No. 14, 2157–2168, 2007.

16. Du, P., B.-Z. Wang, H. Li, and G. Zheng, "Scattering analysis of large-scale periodic structures using the sub-entire domain basis function method and characteristic function method," *Journal of*

Electromagnetic Waves and Applications, Vol. 21, No. 14, 2085–2094, 2007.

17. Fardis, M. and R. Khosravi, "Analysis of periodically loaded suspended substrate structures in millimeter wave," *Progress In Electromagnetics Research B*, Vol. 3, 143–156, 2008.

18. Lu, W. B., Q. Y. Zhao, and T.-J. Cui, "Sub-entire-domain basis function method for irrectangular periodic structures," *Progress In Electromagnetics Research B*, Vol. 5, 91–105, 2008.

19. Saed, M. A., "Reconfigurable broadband microstrip antenna FED by a coplanar waveguide," *Progress In Electromagnetics Research*, PIER 55, 227–239, 2005.

20. Martìn, F., F. Falcone, J. Bonache, T. Lopetegi, M. A. G. Laso, and M. Sorolla, "Analysis of the reflection properties in electromagnetic bandgap coplanar waveguides loaded with reactive elements," *Progress In Electromagnetics Research*, PIER 42, 27–48, 2003.

21. Agilent Genesys EDA Software 2008.07, Agilent Technologies Inc., USA, 2008.